Chemical Engineering Journal 352 (2018) 558–571

Contents lists available at ScienceDirect

Chemical Engineering Journal

journal homepage: www.elsevier.com/locate/cej

A fundamental investigation of gas/solid mass transfer in open-cell foams using a combined experimental and CFD approach

Mauro Bracconi[1], Matteo Ambrosetti[1], Matteo Maestri, Gianpiero Groppi, Enrico Tronconi*

Laboratory of Catalysis and Catalytic Processes, Dipartimento di Energia, Politecnico di Milano, via La Masa 34, 20156 Milano, Italy

HIGHLIGHTS

- Fundamental investigation of external mass transfer in open-cell foams.
- CFD simulations and experiments quantify the effects of morphological parameters.
- New correlation for mass transfer coefficients in foams covers unprecedented range.

GRAPHICAL ABSTRACT

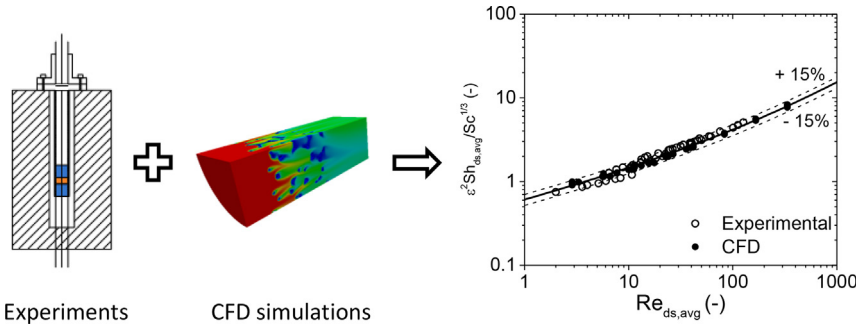

ARTICLE INFO

Keywords:
Open-cell foams
Structured catalysts
Gas-solid mass transfer
Computational Fluid Dynamics
CO oxidation

ABSTRACT

In this work, we combine numerical (CFD) simulations and experimental measurements in a fundamental investigation of the fluid-solid mass transfer properties of open-cell foams, which are promising support for catalytic applications limited by external heat and mass transfer. CFD simulations are exploited to gain insight into the complex transport mechanisms and to enable a parametric analysis of the geometrical features by means of virtually-generated structures. Catalytic activity experiments under diffusion control are used to validate the CFD results and to extend the range of conditions and foam morphologies investigated. Analysis of the flow field by CFD simulations provides a rational basis for the choice of the average strut size as a physically sound characteristic length for mass transfer correlations. Results from both numerical simulations and experimental tests are interpreted according to a fully-theoretically based geometrical model for the prediction of the specific surface area, which accounts for the detailed node-strut geometry. The effects of cell size and strut shape are properly included in the functional dependence of the Sherwood number on the Reynolds number. The effect of porosity requires one additional dependence, wherein the Sherwood number is inversely proportional to the square of the void fraction. The resulting Sherwood–Reynolds correlation is in excellent agreement with experimental data and CFD simulations. It enables accurate (± 15%) estimation of the external mass transfer coefficients for open-cell foams when coupled with the proposed geometrical model from two readily accessible pieces of geometrical information, i.e. the void fraction and either the cell size or the pore diameter of the foam. The derived correlation can be applied to the design of novel enhanced open-cell foam catalyst substrates and structured reactors.

* Corresponding author.
E-mail address: enrico.tronconi@polimi.it (E. Tronconi).
[1] These authors equally contributed to this work.

https://doi.org/10.1016/j.cej.2018.07.023
Received 26 February 2018; Received in revised form 31 May 2018; Accepted 2 July 2018
Available online 05 July 2018
1385-8947/ © 2018 The Author(s). Published by Elsevier B.V. This is an open access article under the CC BY-NC-ND license (http://creativecommons.org/licenses/BY-NC-ND/4.0/).

Notation

Latin letters

d_c	cell diameter [m]
d_s	strut diameter [m]
$d_{s,avg}$	average strut diameter [m]
d_h	hydraulic diameter [m]
d_{Sauter}	Sauter diameter [m]
$d_{eq,corr}$	corrected equivalent diameter [m]
$t_{coating}$	average coating thickness [m]
S_v	specific surface area [m^{-1}]
L	sample length [m]
A	cross-sectional area of the reactor [m^2]
u	empty tube fluid velocity [m/s]
k_{MAT}	mass transfer coefficient [m/s]
$\mathfrak{D}$	diffusivity [m^2/s]

Greek letters

ε	hydraulic void fraction [–]
ρ	fluid density [kg/m^3]
μ	fluid viscosity [Pa s]
ω	mass fraction of externally mass transfer limited species [–]
ω	cup-mix mass fraction of externally mass transfer limited species [–]
χ	conversion [–]

Subscripts

IN	evaluated at the inlet of the reactor
OUT	evaluated at the outlet of the reactor

Superscripts

c	circular cross-section
t	triangular cross-section
bare	referred to bare foam
coated	referred to coated foam

Dimensionless numbers

$Re_{d_{s,avg}} = \frac{\rho u d_{s,avg}}{\mu}$ Reynolds number

$Sh_{d_{s,avg}} = \frac{k_{MAT} d_{s,avg}}{\mathfrak{D}}$ Sherwood number

$Sc = \frac{\mu}{\rho \mathfrak{D}}$ Schmidt number

1. Introduction

The development of structured catalysts for process intensification is a topic of growing interest since several catalytic processes suffer from heat and mass transfer limitations at the industrial scale. For their characteristic features, open-cell foams are regarded as promising innovative substrates for several catalytic processes. In particular, a beneficial effect is expected in applications where external (fluid-solid) heat and mass transport are relevant for the proper design and operation of the reactor. Open-cell foams are cellular materials where interconnected void regions, named cells, are enclosed in a randomly interconnected solid matrix whose solid ligaments, also called struts, converge in nodes; open cells communicate through windows, called pores. These structures are characterized by high void fractions, which allows for low pressure drops even with high flow rates with respect to packed bed reactors. The large specific surface area enables high fluid-to-solid mass transfer rates in the case of catalytically active structures. Moreover, the intricate and complex geometry increases the local mixing and the gas-solid transfer rates, since the struts strongly interact with the flow field resulting in continuous boundary layer formation and disruption, leading to enhanced transport [1–3]. The continuity of the solid matrix in all directions guarantees high axial and radial heat transfer in the case of thermally conductive foams [4] and gas medium. Several potential applications have been investigated in the open literature, mostly addressing NOx removal from vehicle exhaust gas [5]. In exhaust after-treatment applications, the optimal tradeoff between external mass transfer and pressure drop is central. Compared to conventional honeycombs, open-cell foams exhibit higher pressure drops, that hence should be over-compensated by an increase of mass transfer rates. Moreover, open-cell foams usually exhibit higher volumetric mass transfer rates with respect to honeycombs, thus allowing for smaller catalytic converters [1]. At the same time, foams might be a suitable solution also in adiabatic processes where the external transport limitations control the behavior of the reactor, e.g. the highly exothermic catalytic partial oxidation of methane and other hydrocarbons [6,7].

In the literature, several works have investigated gas-to-solid heat or mass transfer in foams, which are governed by the same mechanism, according to the Chilton-Colburn analogy [2].

The analysis of the heat/mass transfer performances of foams requires the definition of a geometrical model, which can describe the complex foam structure. In this regard, the accurate evaluation of the specific surface area is pivotal for further analysis and interpretation of the data. Geometrical models based on the repetitive arrangement of simple unit cells have been derived for the estimation of this property. The first attempts were carried out by exploiting a cubic unit cell [1,2]. Afterwards, more complex and realistic descriptions based on the dodecahedral [8] and tetrakaidekahedral (TTKD) cell have been proposed [9,10]. On the other hand, realistic reconstructions of the foam geometry can be obtained either by tomographic scans of real samples [11–13] or by means of synthetic virtual models [14–21]. The tomographically-reconstructed structures reproduce the real foam geometry providing an accurate estimation of the geometrical properties at the expense of time-consuming procedures and costly machinery. However, the analysis of the tomographic images requires several steps which could introduce errors for volume and surface estimation even increasing the adopted resolution, as pointed out by Heidig et al. [22]. In this view, the values obtained by tomographic measurements require a careful analysis of the results to avoid large errors in the estimates of the geometrical properties. On the other hand, virtual models provide tridimensional reconstructions of the foam structure, but their accuracy relies on the adequacy of the assumptions employed for their derivation. Ordered arrays of unit cells have been proposed employing cubic and tetrakaidekahedral unit cells [19–21]. More accurate descriptions have been obtained from virtual models accounting for the random nature of foams. They rely on randomization of the ordered arrays of deterministic unit cells [18], or spatial tessellations [14–16].

The investigation of the interphase transport phenomena in open-cell foams has been addressed both numerically and experimentally in the scientific literature. In particular, a few papers are available regarding the evaluation of external mass transport via Computational Fluid Dynamics (CFD). Della Torre et al. [20] investigated mass transfer phenomena by considering an ensemble of five regular Kelvin cells in a row. Lucci et al. [18] carried out numerical simulations of external mass transfer in virtual structures obtained by randomizing the perfectly ordered Kelvin structure according to a stochastic displacement of nodes.

More works can be found in the literature regarding gas-to-solid heat transport. Peng et al. [21] proposed a numerical study of convective heat transfer over idealized foam unit cells based on a body-

centered cubic (BCC) packing. De Schampheleire et al. [19] studied fluid dynamics inside idealized open-cell substrates, where single cells were modeled assuming a tetrakaidekahedral cell and parabolic variation of the struts diameter along the axis. The description of the transport properties by means of ordered arrays of unit cells showed unsatisfactory results due to the high degree of order which is not characteristic of real foams. This has been highlighted by Habisreuther et al. [23] for the analysis of the flow field in these structures. Thus, we expect that significant deviations could be obtained in the description of the external mass transfer.

Ambrosio et al. [11] analyzed the heat transfer performances both of ideal minimal surface area Kelvin cells computed with the Surface Evolver software tool and of tomographic reconstructions of real foams. They point out the importance of the proper description of strut cross-sectional shape to properly reproduce the behavior of the real structure. Zafari et al. [12] investigated the effect of the porosity on the external heat transfer by means of CFD simulations on tomographic reconstructions of real foam. Meinicke et al. [13] carried out a detailed investigation of the hydrodynamics and external heat transfer in tomographic reconstructions of open-cell foams. This kind of approach, however, can hardly be used to properly investigate general trends with respect to the effect of the key geometrical properties since it requires the tomography-scan of several real foam samples with a regular variation of the parameters.

From the experimental standpoint, a pioneering work for the evaluation of mass transfer in foams was presented by Richardson et al. [24]. The authors investigated the gas/solid mass and heat transport properties of ceramic foams. Giani et al. [1] and, later, Groppi et al. [25] performed the analysis of mass transfer in open-cell substrates washcoated with Pd/Al_2O_3, running CO oxidation in the diffusion limited regime. Incera Garrido et al. [26] published an experimental investigation of mass transfer in ceramic foams activated with Pt/SnO_2 for CO catalytic oxidation. To explore a wide range of flow rates, the operation of the reactor was either in plug flow configuration or with a recycle. Dietrich et al. [27] investigated the gas/solid heat transfer performances of open-cell foams with a 1-D transient heterogeneous model.

Many of these works were aimed at developing engineering correlations able to describe the gas/solid heat or mass transfer. In particular, Giani et al. [1] proposed a correlation based on the cubic cell model where the strut diameter was chosen as the characteristic length in analogy to tube banks. Groppi et al. [25] revised the latter work using the same assumptions but considering the interstitial velocity in the Reynolds number. Incera Garrido et al. [26] proposed a correlation for the estimation of mass transfer properties of foams in a wide range of porosities based on an idealized TKKD geometry and assuming the sum of the pore and strut diameters as the characteristic length. The proposed correlation includes a non-trivial dependency on the porosity and on the characteristic length. Dietrich et al. [27] proposed a correlation for gas/solid heat transfer based on the hydraulic diameter. Huu et al. [8] published a correlation based on the strut diameter as characteristic length, which includes an additional dependence on the specific surface area. Recently, Reichelt et al. proposed a generalized description of mass transfer in fibrous media where two asymptotic contributions are included [28]. In this study, the authors introduce the Sauter diameter (i.e. $6(1-\varepsilon)/S_v$) as characteristic length.

Despite the considerable amount of experimental and theoretical work, a fundamental understanding of the flow field and the transport properties is still missing. Consequently, a large variety of characteristic lengths has been proposed along with corresponding engineering correlations. However, the predictions of transport properties are still widely scattered.

In this work, we focus on the fundamental analysis of the external mass transfer process by combining both numerical simulations and experimental activity. In particular, a comprehensive investigation of the gas-to-solid transport is carried out, which aims at deriving a reliable correlation for the estimation of mass transfer coefficients. On one hand, experimental evaluation of mass transfer in open-cell foams is performed running CO oxidation over washcoated foams to extend the previously investigated ranges [1]. On the other hand, Computational Fluid Dynamics is employed to increase our understanding of such structures, being able to grant a deep insight in the complex flow field and in the transport mechanism, and to derive lumped transport parameters, as recently shown by Rebughini et al. [29,30]. Hence, simulations of virtually-reconstructed foams [14] facilitate the parametric analysis of the geometrical properties (e.g. effect of porosity, cell size, strut cross-sectional shape) enlarging the range of samples experimentally investigated, as recently shown by Nie et al. [16]. The coupling of numerical and experimental tests enables us to propose the broadest so far reported analysis of mass transfer in open-cell foams. This study shows that external mass transfer phenomena in these structures can be viewed as the interaction of the fluid flow with a set of submerged objects, wherein the struts provide the dominant contribution. As a final result, this work derives a reliable engineering correlation for the description of the external mass transfer in open-cell foams, which covers the widest range of operating conditions and geometrical parameters so far.

2. Methods

In this section, we describe the different methods and modeling approaches employed for the investigation of the mass transfer properties of open-cell foams. As already highlighted in the introduction, we have investigated the external mass transport by means of both experiments and numerical simulations based on Computational Fluid Dynamics. First, the description of the geometrical model exploited for the analysis of both simulations and experiments is presented. Then, the virtual reconstruction procedure is briefly described. Moreover, the adopted CFD model and the experimental setup and procedures are introduced, along with the conventional 1D reactor model exploited for the interpretation of the results.

2.1. Geometrical modeling of open-cell foams

The choice of a proper geometrical model of open-cell foams is crucial to enable a systematic analysis of the transport phenomena. The random nature of open-cell foams is usually described by means of idealized geometrical models, whose mathematical derivations are based on geometrical assumptions or on adaptive coefficients to estimate the properties of open-cell foams. In this regard, Ambrosetti et al. [9] have proposed a fully theoretical derivation of the geometrical properties of open-cell foams based on a tetrakaidekahedral unit cell (TKKD), with struts of variable cross-section, that complies with the Plateau rules and imposes the smoothness of the profile at the node interface. The key geometrical parameter considered in the model is the cell diameter, because it is the size of the single building block of the foam structure and, among all the geometrical properties, it is the one that shows the lowest standard deviation based on the μ-CT analysis. Based on this, the proposed model [9] enables the evaluation of the specific surface area and other key geometrical quantities starting from this directly-measured property along with the porosity (or the relative density). This model has been validated against several experimental measurements of open-cell foams with circular and triangular struts in the widest so far reported range of porosities.

The strut diameter can be calculated for foams with circular or triangular struts starting from the cell diameter and the porosity as the intermediate root of the cubic equations Eqs. (1) and (2) [9].

$$\frac{-0.3985 d_s^{c3} + 2.8803 d_s^{c2} d_c + 0.2172 d_s^c d_c^2 + 0.00708 d_c^3}{0.419 (d_c + d_s^c)^3} = 1-\varepsilon \quad (1)$$

$$\frac{-0.3301d_s^{t3} + 1.4757d_s^{t2}d_c + 0.1871d_s^t d_c^2 + 0.01047d_c^3}{0.419(d_c + 0.\ 577\ d_s^t)^3} = 1-\varepsilon \quad (2)$$

The specific surface area can be calculated as a function of the cell diameter, porosity and strut diameter with Eqs. (3) and (4) [9].

$$S_v^c = \frac{-7.377d_s^{c2} + 10.082d_s^c d_c + 0.3548d_c^2}{0.419(d_c + d_s^c)^3} \quad (3)$$

$$S_v^t = \frac{-5.9960d_s^{t2} + 8.9234d_s^t d_c + 0.5226d_c^2}{0.419(d_c + 0.\ 577\ d_s^t)^3} \quad (4)$$

As already proposed by Giani et al. [1], the configuration of open-cell foams resembles disordered banks of tubes. In view of this analogy, the characteristic length representative of external mass transfer phenomena should be the strut diameter in the case of circular struts and the strut side length in the case of triangular struts. Motivation for this choice will be reported in Section 4.5.

Struts are characterized by a parabolic profile along the axis, which introduces a longitudinal variation of the strut diameter. The diameter of the struts and of the nodes estimated with the model by Ambrosetti et al. [9] changes with the porosity. Thus, we introduce an average strut diameter, calculated as the integral average of the strut diameter over its length. This quantity can be estimated according to Eq. (5) and Eq. (6) for circular and triangular struts, respectively.

$$d_{s,avg}^c = 0.965d_s^c + 0.0314d_c \quad (5)$$

$$d_{s,avg}^t = 0.965d_s^t + 0.0544d_c \quad (6)$$

The average strut diameter and the surface to volume ratio are respectively directly and inversely proportional to the cell diameter. Accordingly, dimensionless quantities d_s/d_c and $S_v\ d_c$ can be plotted in function of the porosity, as shown in Fig. 1(a) and (b). It is evident from Fig. 1(a) that both the average strut diameters for circular and triangular geometry decrease almost linearly with the void fraction. At fixed porosity, the characteristic length of the triangular-shaped struts is greater than the corresponding characteristic size of the circular struts. The non-dimensional specific surface area decreases with increasing ε as shown in Fig. 1(b). In the case of foams with circular struts, the dashed lines elucidate the contributions of nodes and struts while in case of triangular struts the entire exposed surface is attributed to the struts since the tetrahedral nodes do not expose external surface. A sensitivity analysis has been carried out to quantify the effect of the uncertainties of the experimentally measured geometrical properties, i.e. cell diameter and relative density (1−ε), on the average strut size and on the specific surface area. A ±10% relative deviation of the cell diameter results in the variation of $d_{s,avg}$ and S_v equal to ±10% and ∓10%, respectively. Instead, a relative variation of ±5% of the relative density induces a deviation of $d_{s,avg}$ and S_v equal to ±5% and ±2.5%, respectively.

2.2. Virtual foam reconstruction

The CFD simulations are carried out on a previously proposed virtual reconstruction of open-cell foams, which fully retains the geometrical and fluid-dynamic properties of real open-cell foams [14]. The reconstruction procedure relies on a few pieces of easily accessible geometrical information, e.g. cell diameter, strut cross-sectional shape and porosity. Based on this information, the foam structure is generated according to a Voronoi-tessellation procedure, briefly summarized in the following. The initial seeds required by the algorithm are obtained by means of a random packing of spheres of cell diameter size obtained by a discrete element method. Once the spheres are settled, the centers are extracted and imported in the Voronoi algorithm, which generates the foam skeleton. The accurate description of the strut and node geometries is crucial to capture the transport phenomena prevailing inside open-cell foams. For this purpose, the same geometrical models described in Section 2.1 are adopted according to the theoretical derivation by Ambrosetti et al. [9] as initial guesses which are then refined in order to reach the desired porosity value. More details on the procedure can be found elsewhere [14]. The virtually generated foams have shown a good agreement with experimental measurements for both the geometrical properties and the pressure drop. Moreover, the virtually-generated foams retain the topological properties of real foams, e.g. number of openings in each cell, angle between struts, pore size distribution. Hence, they are able to reproduce the structure of open-cell foams along with the local irregularities in the solid matrix. Additionally, the predictions of the geometrical model [9] are in line with the results of the reconstruction, thus the relationships between the geometrical properties (e.g. cell, pore, strut, node diameters, porosity and specific surface area) presented in Section 2.1 are still valid. The virtual reconstruction enables to simulate data obtained with real foams starting from simple measurements (i.e. cell diameter and porosity). In addition, this procedure combined with CFD enables the parametrical investigation of the effects of the key geometrical quantities on the transport properties in open-cell foams.

2.3. Experimental mass transfer tests

To evaluate the external mass transfer properties, catalytic combustion of CO is chosen as a model reaction, as already proposed in

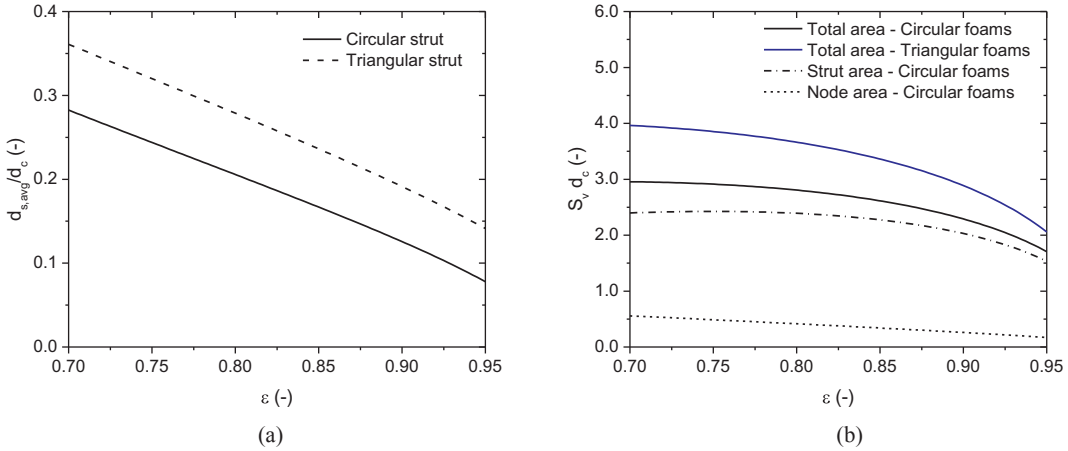

Fig. 1. Non-dimensional characteristic length of circular struts foams and triangular struts foams as a function of the porosity (a) and non-dimensional specific surface area of circular struts foams and triangular foams as a function the porosity; for circular foams the two contributions of the struts and the nodes are reported with dashed and dotted line respectively (b).

earlier work [1,25]. In fact, CO oxidation over noble metals is a fast reaction, which readily reaches a full diffusional control at relatively low temperatures. Moreover, it is fully selective to CO_2. To make them catalytically active, the tested foam samples are washcoated with Pd/CeO_2. The catalytic activation step is a critical part of the process enabling the experimental evaluation of the mass transfer properties of open-cell foams: in this work, spin coating is chosen as the deposition technique, since it was demonstrated to be able to coat uniformly the foam surface. Multiple deposition steps are performed to achieve a uniform loading on the structures and a constant washcoat thickness. Being operated in mass transfer regime, a fundamental requirement is the complete activation of the surface. A visual inspection of the foam samples via optical microscopy reveals that the coating is uniformly distributed and no pores are closed. Further details on the activation of the foam samples can be found elsewhere [31].

To account for the effective geometrical properties of the supports after the washcoating process, the conventional measurement of hydraulic porosity with picnometry is not effective, since ethanol can penetrate the pores of the washcoat resulting in a wrong estimate of the void fraction. The volumetric loading is therefore estimated from the mass load knowing the total porosity of the sample and the density of the coating, evaluated by the analysis of washcoat thickness on stainless steel slabs washcoated with spin coating and, then, by assuming a constant washcoat thickness on the surface. The average coating density for the chosen catalytic powders is estimated to be equal to 2.1 g/cm^3. The geometrical properties of the coated foams can be estimated under the assumptions that a uniform coating thickness is loaded on the structure and that the strut cross-sectional shape is preserved. Thus, the coating thickness ($t_{coating}$) can be evaluated once the porosity of the sample after the coating process (ε_{coated}) is estimated.

An average coating thickness is calculated via Eq. (7)

$$t_{coating} = d_{s,avg}\left(\left(\frac{1-\varepsilon_{coated}}{1-\varepsilon_{bare}}\right)^{0.5} - 1\right) \tag{7}$$

The cell diameter can be easily re-evaluated as reported in Eq. (8)

$$d_c^{coated} = d_c^{bare} - 2t_{coating} \tag{8}$$

The foams samples used in this work are reported in Table 1 and listed from A to C. In particular, the deviation of the geometrical properties from bare (in brackets) to washcoated geometry can be evaluated. A limited variation in the porosity has been induced by the coating procedure. To investigate different flow regimes, CO oxidation in air and CO oxidation in a He/O_2 95/5% mol/mol mixture was performed at different flow rates in the range of 1–25 Standard Liters per Minute (SLM – @ 298 K - 1 bar) for air and 3–9 SLM for the mix. Replacing N_2 with He/O_2 mixture at the same molar flow rate enables to extend the analysis to the low Reynolds regime since its density is almost one order of magnitude less than the air density. More details of the conditions used in experimental tests are reported in Table 2.

The gases are pre-heated and mixed in an electrically-heated coil before entering in the reactor, as already described by Giani et al. [1]. Two different gas analyzers are used for the measurement of reactants and products compositions, namely a HP Agilent 6890 GC and a Pollution micro-GC both equipped with columns functionalized with molecular sieves and Porapack and equipped with thermal conductivity detectors (TCD). Internal standards are adopted, in particular nitrogen and helium are chosen for the two different test campaigns. The error in the carbon balances was lower than 5% in all the experimental tests. In this work, catalytic foam samples with a diameter of 9 mm and different lengths (see Table 1), are loaded in a tubular microflow reactor placed in a vertical oven with the same geometry described in Giani et al. [1]. The sample length is chosen in order to ensure both the presence of at least of three cells in the axial direction, as recommended by Bianchi et al. [4], and CO conversions lower than 98%. In a typical experiment, the oven set temperature is incremented stepwise until the diffusional regime is reached. The catalyst is operated under a slight overpressure to fill the sampling valves of the GC. Noteworthy, the pressure has no influence on the conversions in the mass transfer limited regime and on the dimensionless Sherwood number. To guarantee a uniform flow field and to avoid maldistributions, additional bare foams were added upstream and downstream of the catalytic sample. For the correct evaluation of the transport properties, a pressure gauge was used to record the pressure in the reactor, while the temperature at the inlet and at the outlet of the catalytic bed is measured with K-type thermocouples. In order to evaluate the reproducibility of the measurements, each condition is tested at least 3 times and is considered when deviations in the measured conversion are lower than 0.2%. After the complete experimental campaign, selected tests were repeated to assess any possible deactivation due to possible coating detachment. Different CO feed concentrations (from 1 to 3%) have been tested, with the aim both to confirm the achieved mass transfer regime and to find an optimal feed CO concentration able to ensure high precision in the evaluation of the products compositions and to reduce the temperature rise in the catalytic sample. The CO conversion in the asymptotic high-temperature regime has been proven to be independent of the CO concentration and the CO content in the feed is fixed to 1.5% v/v for the entire experimental campaigns. In these conditions, a maximum temperature difference of 80 °C is measured between the inlet and the outlet of the catalytic bed.

2.4. CFD modeling

The CFD simulations are carried out by means of catalyticFoam [32], a numerical framework able to couple the accurate solution of the Navier-Stokes equations and of the species mass balances with the detailed characterization of the surface chemistry. A detailed description of the mathematical model and of the numerical methods employed for the solution is reported by Maestri et al. [32] along with an extensive validation of the proposed methodology. The diffusive limitations inside the catalytic coatings are deemed to be negligible, and the reaction rates at the washcoat surface are assumed to equal the local diffusive species mass fluxes. In this work, we focus our attention on the investigation of gas-to-solid mass transfer properties, thus the simulations are carried out in the external mass transfer fully limited regime. This is achieved by imposing infinitely fast heterogeneous reactions to reach a null surface concentration of the mass transfer limited reactant. A second-order upwind scheme (linear upwind) was adopted for the discretization of the convective terms, while a pure second-order scheme was employed for the diffusive terms.

The computational domains were generated starting from the CAD file, generated by the foam reconstruction procedure, by means of the

Table 1
Geometrical features of the open-cell foams exploited for experimental tests in this work (A–C) and in [1] (D–F). Geometrical properties used for the evaluation of mass transfer properties and of bare foams (in brackets).

Foam sample	d_c [mm]	ε_H [–]	S_v [m^{-1}]	$d_{s,avg}$ [mm]	L [mm]
A[b,c]	0.625 (0.643)	0.880 (0.915)	4973 (4185)	0.117 (0.099)	1.90
B[a]	3.520 (3.538)	0.890 (0.898)	673 (647)	0.472 (0.450)	10.00
C[b]	3.600 (3.686)	0.915 (0.923)	745 (699)	0.530 (0.490)	12.70
D[b,c] [1]	2.000	0.937	1163	0.238	12.50
E[b,c] [1]	1.700	0.932	1425	0.214	6.25
F[b] [1]	4.700	0.927	533	0.624	25.40

[a] Strut with circular cross-sectional shape.
[b] Strut with triangular cross-sectional shape.
[c] Foam structure for the CFD simulations of the validation of the virtually-generated structures.

Table 2
Operating conditions in experimental test for estimation of mass transfer coefficients.

Feed temperature		573–723	[K]
Outlet pressure		1.4	[bar]
Feed mass fraction	CO	0.015	[–]
Test in Air	N2	0.778	[–]
	O2	0.207	[–]
Test in He/O2	He	0.936	[–]
	O2	0.049	[–]
Reynolds number		1–130	[–]

snappyHexMesh utility of the OpenFoam framework. The computational domain is generated starting from a background mesh with a ratio between the foam cell diameter and grid size of 20. To accurately describe the boundary layer, a level of refinement equal to 4 around the surface is adopted, which guarantees a y + value around 1 in each flow condition. The insertion of prism layers around the surface is not needed because of the low Reynolds number of the simulation [33]. Details on mesh generation, convergence analysis and numerical setup of the simulations are reported in the Supplementary Material.

2.5. 1D foam reactor model

Both numerical and real experiments were analyzed by a conventional 1D heterogeneous steady-state isothermal plug-flow reactor model. Under the assumption of full external mass transfer control, the differential mass balance for the limiting reactant can be expressed as follows:

$$-u\rho\frac{d\omega}{dz} = k_{MAT}S_v\rho\omega \tag{9}$$

Eq. (9) is derived assuming a uniform flow distribution and constant transport properties due to the diluted conditions of both the numerical simulations and the experimental runs. The foam specific surface area S_v is evaluated using the ideal TKKD model described in Section 2.1. By introducing the Sherwood number (see Notation for definition), Eq. (9) can be reformulated as follows:

$$-u\rho\frac{d\omega}{dz} = \frac{Sh_{d_{s,avg}}\mathfrak{D}}{d_{s,avg}}S_v\rho\omega \tag{10}$$

On integrating Eq. (4) over the length of the reactor (z = L) and solving for Sh_{d_s}, we obtain:

$$Sh_{d_{s,avg}} = -\frac{d_{s,avg}u}{\mathfrak{D}S_vL}\ln\left(\frac{\omega_{OUT}}{\omega_{IN}}\right) \tag{11}$$

By introducing the definition of conversion χ:

$$Sh_{d_{s,avg}} = -\frac{d_{s,avg}u}{\mathfrak{D}S_vL}\ln(1-\chi) \tag{12}$$

In the case of the experimental tests, the measured inlet and outlet CO concentrations have been used for the evaluation of the conversion. In the case of CFD simulations, the conversion is evaluated on the basis of ω_{OUT} and ω_{IN} which are computed as the cup-mix average [34] values, estimated according to Eq. (13)

$$\widetilde{\omega}_{OUT/IN} = \frac{\int_A \rho\omega u dA}{\int_A \rho u dA} \tag{13}$$

The thermodynamic and transport properties adopted in this work for the analysis of the CFD and experimental data and for the CFD simulations are evaluated by means of the OpenSMOKE++ libraries [35]. In particular, the thermodynamic properties of the gas species, estimated following the approach proposed by Gordon and McBride [36], are exploited to calculate the gas mixture properties using the Gibbs theorem. The transport properties are evaluated according to standard kinetic theory expressions [37,38].

3. Experimental results

This section reports the results of new dedicated mass-transfer limited CO oxidation tests, which extend the experimental coverage of mass transfer phenomena to foams with higher cell densities and in a wider range of Reynolds numbers than so far available in the literature.

3.1. CO light-off curves

Examples of CO conversion curves in function of the catalyst temperature are displayed in Fig. 2. Conversion curves show a similar light-off trend on increasing temperature: negligible conversion at low temperatures, then ignition and, finally, a plateau where the conversion is no longer influenced by the temperature. The temperature independent asymptote confirms the shift from the chemical regime, where the conversion grows exponentially with temperature, to the physical regime associated with a small dependence on temperature. Fig. 2(a) shows the effect of the flow rate on the CO conversion in air. The conversion clearly decreases with increasing flow rate, due to the decrement of the residence time. The effect of the mixture properties can be inferred as well from Fig. 2(b). CO conversions are higher in strong helium dilutions. This is justified by the fact that the CO diffusivity is almost twice the value in air. This effect is strong enough to

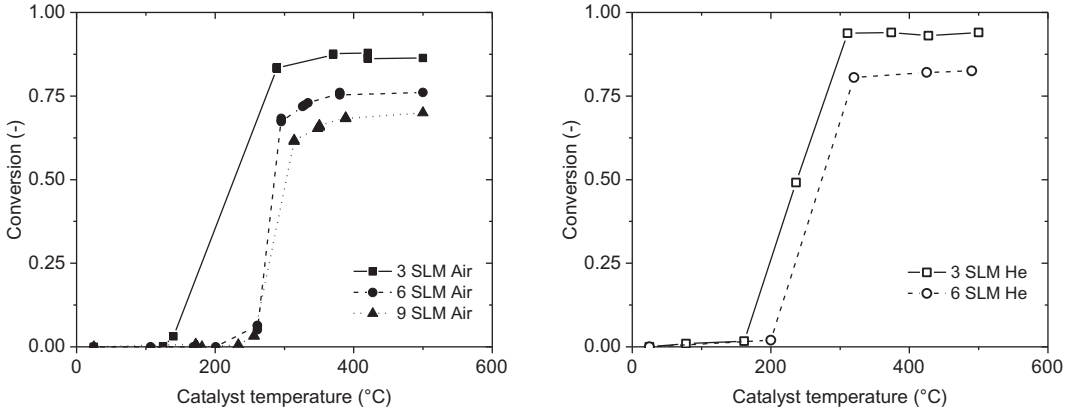

(a) (b)

Fig. 2. Conversion curves for foam B in air and mixture at different flow rates: conversion curves in air at 3, 6 and 9 SLM (a); conversion curves collected in helium/oxygen mix at 3 and 6 SLM (b).

compensate the decrease in the Reynolds number due to the lower density of the feed.

3.2. Experimental study of mass transfer at low Reynolds numbers

In this paragraph, we focus on the experimental evaluation of mass transfer properties at low Reynolds numbers. The so far available literature correlations for mass transfer in foams are valid for Re greater than 10, while one of the objectives of this work is the evaluation of mass transfer properties at low Reynolds numbers so to extend the existing correlation range. As already mentioned in the discussion of the methodologies, in this work two different approaches have been introduced for this purpose. The analysis of the mass transfer properties of high cell density foams (Foam A) has been coupled with the analysis of mass transfer in a stream with a high dilution of Helium (Foam B and C). Dealing with such small dimensions, the impact of the coating on the geometrical properties needs to be accounted for, as already pointed out in Section 2.3.

Fig. 3 shows the results in the range $1 < Re < 10$ in terms of a Sherwood-Reynolds dimensionless log-log plot. Note that the plotted Sherwood numbers are divided by Schmidt number at power 1/3, as typically reported in literature. An assessment of this choice is presented in the Supplementary Material. The data fall essentially on a straight line, with limited deviations which can be explained by the experimental error in presence of very high conversions occurring at very low Reynolds. A slope of the Sherwood number equal to 1/3 with respect to the Reynolds number is apparent. This confirms the analysis proposed by Reichelt et al. [28] in analogy with random beds of spheres. Our results are also consistent with the work of Ishimi et al. [39] which theoretically investigated viscous creeping flow in tube banks by means of the free surface model [40], finding that the Sherwood number depends on the Reynolds number raised to a power of 1/3.

Hence, a viscous flow term with an exponent of the Reynolds number equal to 1/3 should be included in the correlation in contrast with previous correlations developed the description of mass transfer in open-cell foams [1,26]. These correlations were based on experimental data collected at higher Reynolds numbers characterized by different flow regimes.

3.3. Experimental study of mass transfer from intermediate to high Reynolds numbers

The experimental investigation is then extended to the entire range of achievable Reynolds numbers allowed by the adopted experimental setup. The results are shown in the dimensionless form in Fig. 4. The small cell and strut diameters which characterize Foam A determine that the maximum Reynolds number for this foam sample is in the laminar regime ($Re < 30$). Foams B and C, characterized by struts with circular and triangular shape respectively, are tested from the low Re regime to Reynolds numbers up to 100. These foams show performances close to the results reported by Giani et al. [1] who investigated a similar range of Re, although on foams with different cell diameters. This aspect is crucial, stating that the observed influence of the cell diameter can be correctly accounted for by the combination of geometrical model and characteristic length assumed in the present work.

Despite the difference in the shape of the strut, the Sh vs. Re curves of foams B and C are almost superimposed in the entire range of Re. The adoption of the TKKD model [9] and the choice of the average strut diameter as the characteristic length align these data and, hence, enable the development of a single correlation which can faithfully describe the mass transfer properties of foams with both circular and triangular struts.

Notably, the log-log plot of the Sherwood number against the Reynolds number in Fig. 4 shows a different exponential dependence than in Fig. 3, due to the shift from fully laminar to the transitional flow regime. As already reported by Reichelt et al. [28], two distinct flow regimes are present in porous media like foams or fibers. A fully laminar and a dissipative regime have to be both accounted for the correct description of mass transfer coefficients in a wide range of Reynolds numbers.

4. Numerical results

In this section, the analysis of CFD simulations is presented to parametrically investigate the effect of the foam morphological properties on the mass transfer phenomena.

4.1. Definition of REV

A parametric analysis of mass transfer requires the definition of the representative volume able to properly describe the foam behavior. The effect of local irregularities characteristic of the complex foam geometry is averaged and becomes negligible considering a sample larger than the representative element volume (REV) [41]. Thus, the definition of the REV is crucial to obtain reliable results from CFD simulations. The REV usually proposed in the literature consists of at least three cells in each direction and it is obtained by achieving sample-independent results for the geometrical properties and pressure drop [4,41]. In this view, several sample sizes have been investigated by changing the number of foam cells in the stream-wise and transversal directions. The computational domains employed in this analysis are described in the Supplementary Material where additional details on the boundary conditions can be found as well. The simulations are carried out isothermally with the operating conditions listed in Table 4. The Sherwood number obtained from the simulation is plotted against the Reynolds number for different foam sample sizes in Fig. 5. The analysis has been carried out starting with the minimum REV proposed in the literature, able to reproduce the geometrical properties of foams [41], and increasing the size in both the stream-wise and the transversal direction to understand the effect of the sample dimensions on the gas-to-solid mass transfer properties. The effect of the length has been investigated by changing the number of open cells in the stream-wise direction, ranging between 3 and 10. The effect of the number of cells in the transversal direction is studied considering samples with a size of 3 and 5 cells. The analysis shows that the REV corresponds to a cube of 3 cells in each direction whatever Reynolds number is considered. This result points out that the entry length in open-cell foams is limited due to the strong mixing effect provided by the interaction with the cellular

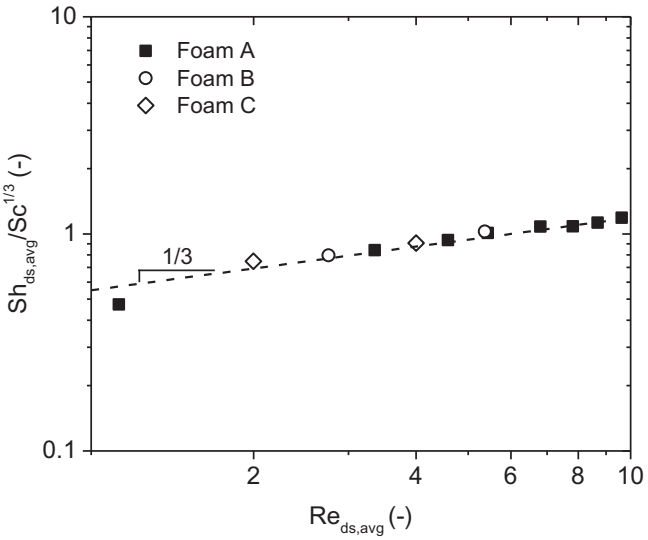

Fig. 3. Experimental evaluation of mass transfer at low Reynolds numbers in air (full symbols) and in helium (empty symbols).

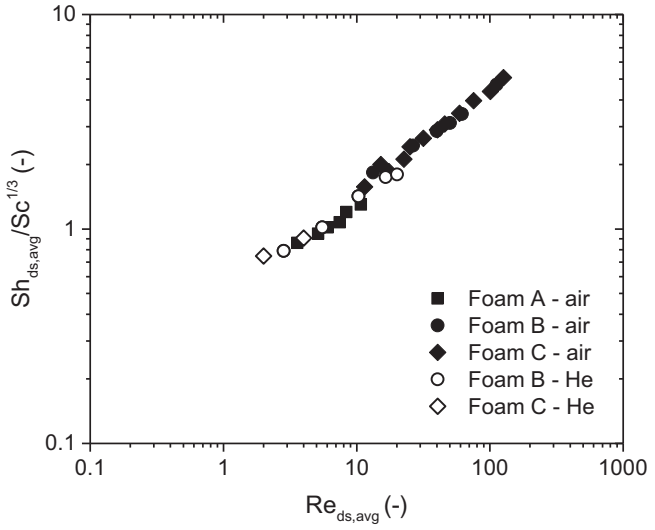

Fig. 4. Complete set of experimental results presented in this work for foam A (square) in air, foam B (circle) and C (diamond) in helium (empty symbols) and air (full symbols).

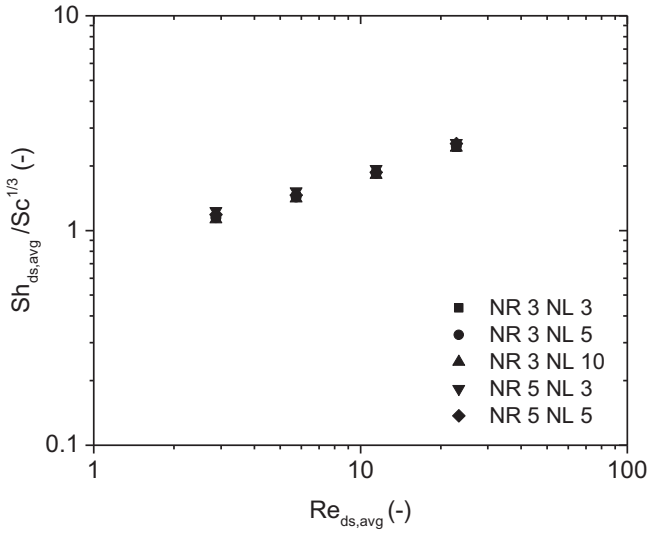

Fig. 5. Effect of the sample size on the prediction of the Sherwood number with respect to different stream-wise (NL) and transversal (NR) number of open cells.

matrix.

4.2. Validation with experimental data

The adequacy of the Voronoi-based reconstruction in reproducing the mass transfer properties of foams has been verified by direct comparison with experimental data from Giani et al. [1] and with novel experiments carried out in this work.

The foams have been reconstructed based on the experimental measurements of the cell diameter and the void fraction. The samples employed in the geometrical validation are larger than the minimum REV and their geometrical information is reported in Table 1. The mass transfer simulations are carried out isothermally under full external mass transfer limitations at the same operating conditions employed in the experiments and reported in Table 2. The capability of the reconstructed foam in the description of the transport properties has been assessed by comparing the experimentally measured CO conversions with those evaluated by postprocessing CFD simulations. Thus, the computational domain reproduces the geometry of the reactor and of

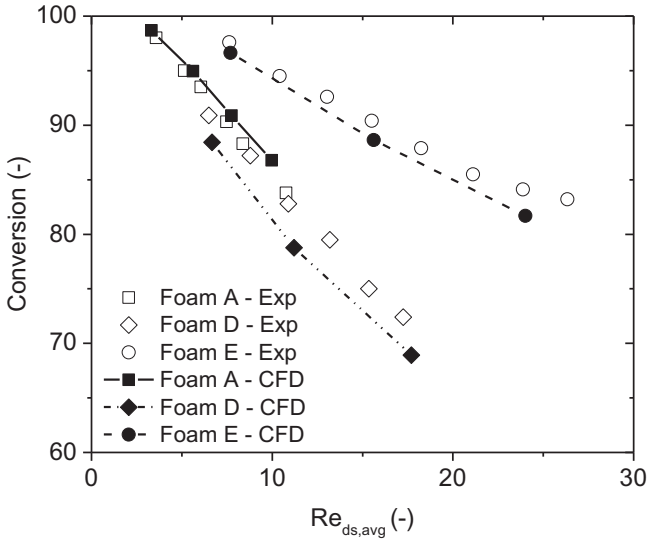

Fig. 6. CO conversion with respect to the Reynolds number based on the strut diameter (empty symbols – experimental data, line and full symbols – CFD simulation).

the foams investigated in the experimental tests, by adopting the same size for the reactor diameter and foam length. Additional details on the computational domain can be found in the Supplementary Material.

Fig. 6 shows the plot of the conversion versus the Reynolds number based on the average strut diameter. The mean absolute percentage error (MAPE) has been evaluated to quantitatively measure the deviations between numerical and experimental data. The conversions predicted by the CFD model are in good agreement with the experimental data. The results of the CFD model are superimposed for Foam A, whose cell diameter and porosity were evaluated after coating, thus allowing for a faithful reproduction of the real sample by means of the synthetic Voronoi foam. This is witnessed by the MAPE value, which is equal to 1.2%. A slight underestimation is noted for Foam D and E, for which the geometrical properties of the bare foams have been considered since no information on the washcoated geometry are available. The MAPE for these two samples is equal to 4.1% and 2.1%, respectively. Nevertheless, the geometry of the coated foams is close to the bare one and only small underestimation on the conversion are observed. These results are in line with the expected effect of the washcoat which increases the specific surface area leading to higher mass transfer rates and, hence, higher conversions than in the bare foams.

As a whole, the results clearly confirm the consistency of the numerical experiments on the Voronoi-based foams with the real ones.

4.3. Effect of porosity

The flexibility of the virtual reconstruction approach allows for the parametric investigation of the effect of the geometry of the foams. As shown in Table 1, foams available for the experiments have similar porosities, thus the effect of the porosity on the mass transfer properties is better investigated by a parametric analysis on the virtual foam structures. Four different void fractions have been considered from 0.7 to 0.95 to analyze the entire range of porosity characteristic of foams. To remove the dependence on the cell size and on the strut shape, these geometrical properties have been kept constant. In particular, the cell size has been assumed equal to 1.0 mm and a circular cross-sectional shape has been considered, while the required porosity is achieved by changing the node and strut size. Table 3 lists the geometrical properties of these structures.

The simulations are carried out at the operating conditions listed in Table 4 defined to achieve negligible variations of the transport and thermodynamic properties in the reactor, which are assumed equal to

Table 3
Geometrical features of the virtually-generated open-cell foams exploited for CFD numerical simulations.

Foam sample	d_c [mm]	ε [–]	S_v [m^{-1}]	d_s [mm]	L [mm]
G[a]	1.000	0.700	2955	0.283	3.00
H[a]	1.000	0.800	2806	0.206	3.00
I[a]	1.000	0.900	2290	0.126	3.00
L[a]	1.000	0.950	1705	0.078	3.00
M[a]	0.300	0.900	7634	0.038	0.90
N[a]	1.000	0.900	2290	0.126	3.00
O[a]	2.000	0.900	1145	0.252	6.00
P[a]	3.000	0.900	763	0.377	9.00
Q[b]	2.000	0.900	1443	0.330	6.00

[a] Strut with circular cross-sectional shape.
[b] Strut with triangular cross-sectional shape.

the average value within the foam sample. The empty tube velocity is conveniently modified to span a wide range of Reynolds numbers between 3 and 320. The results are shown in Fig. 7(a) and confirm the possible effect on the mass transfer. At fixed Reynolds number, the Sherwood number decreases on increasing the porosity. The effect of bed voidage is highlighted by plotting the Sherwood number against the void fraction, as in Fig. 7(b). For the four chosen Reynolds numbers, the Sherwood number plotted against the void fraction results in parallel lines with slope equal to −2 in the logarithmic plot.

It is worth to emphasize that the effect of the porosity in these complex and intricated structures strongly depends on the geometrical model employed for the evaluation of both the characteristic length and the specific surface area. Other authors tried to correlate the mass transfer with the foam void fraction, with different results. Incera Garrido et al. [26] proposed a dependence of the Sherwood number on the void fraction equal to $\varepsilon^{0.44}$ assuming the pore diameter as characteristic length. However, their correlation of the Sherwood number comprises an additional term function of the pore diameter, which introduces a further dependence on the void fraction which can be hardly quantified. Zafari et al. [12] obtained a dependence of the Nusselt number on the porosity equal to ε^{-3} by fitting the simulation results on foams of three different porosities. They employed the square root of the permeability as characteristic length, which is a function of the porosity as well. Recently, Reichelt et al. [28] proposed that the effect of the porosity is described by a complex analytical function proposed by Pfeffer [42] for packed beds of spheres when the Sauter diameter is assumed as characteristic length. They further claimed that the external mass transfer in both packed beds and open-cell foams can be described by a single correlation with a scatter at most of 50%. From our simulations, the ε^{-2} dependence better reconciles the data than the Pfeffer function [42], which was originally derived for spheres.

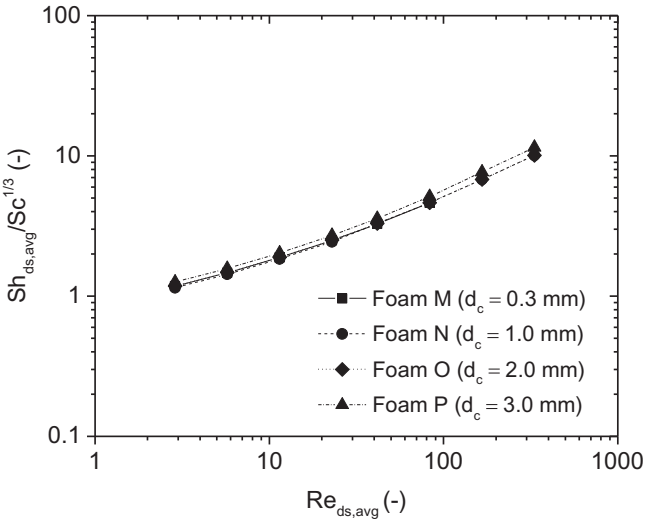

Fig. 8. Sherwood numbers with respect to the Reynolds number for different foam sample characterized by a porosity of 0.9, cylindrical strut and four different cell sizes (square 0.3 mm – diamond 1.0 mm – circle 2.0 mm – triangular 3.0 mm).

4.4. Effect of cell size

The effect of the cell size on the foam mass transfer properties has been investigated by considering four foam samples characterized by different cell sizes at constant porosity ($\varepsilon = 0.9$). Cell sizes between 0.3 mm and 3 mm have been investigated to screen a wide range of different PPIs (Table 3). Fig. 8 shows the effect of the cell diameter on the Sherwood number, according to simulations carried out at the conditions reported in Table 4. It is evident that the effect of the cell diameter on the Sherwood number is negligible at fixed Reynolds number. Moreover, both the characteristic length, i.e. the average strut diameter, and the specific surface area are linearly dependent on the cell diameter, according to the geometrical model proposed by Ambrosetti et al. [9]. The Sherwood number is therefore independent of the PPI at fixed void fractions. This aspect has been already shown by Giani et al. [1], whose Sherwood number data for foams with very similar porosities but different cell sizes are overlapped in Sherwood

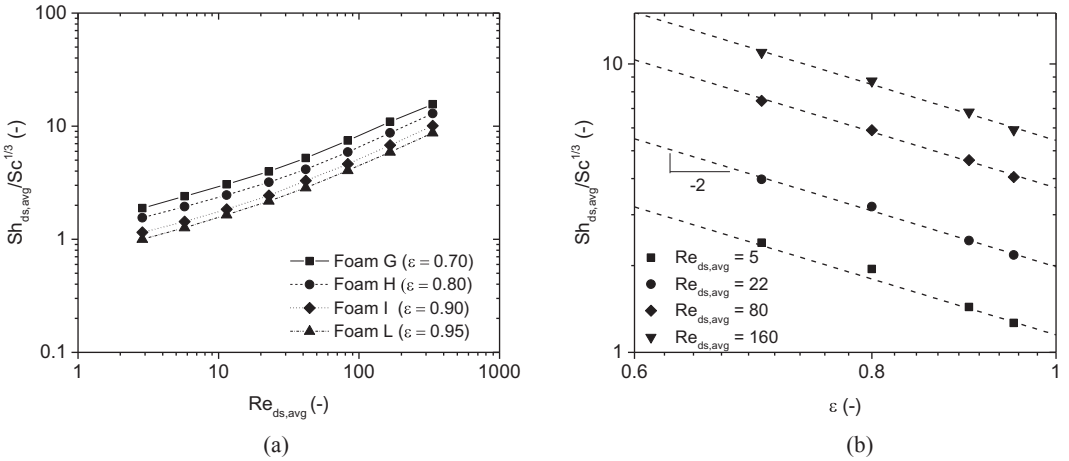

Fig. 7. Sherwood numbers with respect to the Reynolds number for different foam sample characterized by 1 mm cell size, cylindrical strut and four different porosities (0.7 square – 0.8 circular – 0.9 diamond – 0.95 triangular) (a); dependence of the mass transfer coefficient with respect to the void fraction for different Reynolds number (5 square – 22 circular – 80 diamond – 160 triangular).

versus Reynolds plots, once the strut diameter is chosen as the characteristic length, and is further confirmed in this work from the experimental standpoint (Section 3). Notice that the adoption of different characteristic lengths as proposed by Incera Garrido et al. [26] and by Dietrich et al. [43] results in correlations which require additional empirical parameters to describe the experimental data for gas-to-solid mass and heat transfer, respectively.

4.5. Effect of the strut cross-sectional shape

The assessment of the effect of this geometrical parameter is investigated by the virtual generation of two foam samples which share the same cell diameter, porosity and foam skeleton. The difference between the two samples is related to the topology and geometry of strut and nodes. Cylindrical struts with truncated spheres in the nodes are adopted in the case of circular cross-section, whereas struts with triangular shape and tetrahedral node are considered for the triangular cross-section. It is worth to emphasize that the virtual generation procedure relies on the same initial seeds and properties, and solely the strut shape is changed. In this view, the effect of the strut shape is decoupled from the other contributions, allowing for the accurate analysis of its effect. The results of simulations carried out at the conditions of Table 4 are shown in Fig. 9. The Sherwood numbers computed for the two geometries are superimposed at fixed Reynolds and show the same trend. Deviations at most of 2% are experienced at high flow velocities. This is confirmed by the experimental tests reported in Section 3. Moreover, this agrees with the analysis of a single submerged body in cross-flow where the dimensionless transport properties assume the same value in the range of Reynolds of interest, regardless of the shape of the body [44], by adopting as characteristic length the diameter of the cylinder and the length of the lateral side of the triangle instead of the equivalent diameter.

5. Discussion

In this Section, we discuss the choice of the average strut size as the characteristic length for the description of the transport properties in foams. Then, we develop a comprehensive engineering correlation for the description of mass transfer in catalytic foams over a broad range of both flow rates and geometrical properties and, finally, we compare the performances of open-cell foams against conventional structured supports in the mass transfer regime.

5.1. Assessment of the characteristic length

Following the approach adopted in this work, the geometrical characterization of open-cell foams requires the direct measurement of the porosity and of the cell (or pore) diameter. Based on these quantities, all the other geometrical properties (e.g. strut and node diameters, specific surface area) can be evaluated according to a geometrical model. In principle, all these geometrical sizes, either directly measured or estimated according to a geometrical model, could be employed as characteristic length.

We tackle the problem of the identification of the characteristic length by analyzing both the morphology of foams and the mechanism of the interaction between the fluid and the solid matrix. Open-cell foams usually exhibit two different strut cross-sectional shapes depending on the porosity, see Table 1. Until porosities around 0.9, the strut shape is typically circular, whereas for higher porosities a triangular shape is found [10]. For extremely high porosity ($\varepsilon > 0.96$), a triangular concave cross-section is obtained [10]. In this work, we focus on cylindrical and triangular cross-sectional shapes which are common in the range of porosity of interest for catalytic applications.

Our characteristic length is the average strut size, which is the length integral average side of the triangle or the diameter of the cylinder in the case of triangular or circular cross-sectional shape, respectively (see Section 2.1). This choice is in line with our previous work [1], where the strut diameter was proposed in analogy with the assumption of the tube diameter for the heat transfer in banks of tubes. The average strut size is, in fact, analogous to common choices adopted in the heat transfer literature to analyze flow around submerged objects, like a single cylinder or tube banks. In fact, in the case of open-cell foams the average strut size is able to describe the transition between the Darcy and the post-Forchheimer flow regime, as shown by the appearance of vortexes detached from the submerged struts, around the same Re values reported in the literature for cylinders with triangular and circular cross-sectional shapes. The complex nature of the tridimensional structure of open-cell foams hinders the accurate definition of such a transition Reynolds number. However, the non-stationary phenomena, typical of the post-Forchheimer regime, become evident around a Reynolds number based on the average strut size close to the literature value for submerged bodies in cross flow. Fig. 10 shows the flow field around one strut within the foam structure. At low Re, the fluid flow around the object is typical of the fully laminar regime, with the streamlines surrounding the submerged body. At higher Re, the onset of flow instabilities is evident. Vortices are present after the strut and the detachment of vortexes is experienced starting from Re around 40, i.e. in good agreement with the literature flow around banks of tube and submerged cylinders [45]. A further increase of Re determines a different pattern for the wake. It is worth to emphasize that at this Re the flow field within the open-cell foam is still laminar and the simulations can be carried out assuming laminar conditions without losing in accuracy [46,47]. A fully rigorous correspondence with bundles of tubes is not appropriate, due to the obviously different morphology of open-cell foams, where the struts are randomly oriented and join in nodes. However, the struts are the primary structures involved in the external transport phenomena. They are responsible for the dominant contribution to the total superficial area, as shown in Fig. 1(b), since almost the 85% of the exposed area belongs to the struts. Moreover, the analysis of the distribution of the local mass flux reveals that the struts account for more than the 90% of the overall diffusive flux. The complex structure of the foam and the arrangement of the struts determine that the ligaments are the region more exposed to fluid and, thus, to the fluid-solid mass transfer. These results make the analogy with bundles of tubes still effective.

The average strut size also enables to drop the dependence on the strut cross-sectional shape in the evaluation of the Sherwood numbers, as reported in Section 4.5, leading to a unique description whichever strut cross-sectional shape is considered.

As a matter of fact, there is still no consensus on the definition of the characteristic length of open-cell foams. Several proposals are found in the literature. The square root of the permeability coefficient [21] has been suggested in analogy with porous media. It can be estimated as a complex function of the void fraction and of the strut diameter, being these quantities involved in the viscous contribution of the Darcy-Forchheimer equation [48]. Thus, this entity comprises a non-trivial additional dependence on the void fraction. Differently, Dietrich et al. [43] recommends the hydraulic diameter (Eq. (14)) as the characteristic length for the description of both pressure drop and gas-to-solid heat transfer,

Table 4
Operating conditions for CFD parametric analysis of the geometrical features of mass transfer.

Feed temperature		298	[K]
Outlet pressure		1.4	[bar]
Feed mass fraction	reacting species	0.03	[–]
	inert	0.97	[–]
Reynolds number		3–320	[–]

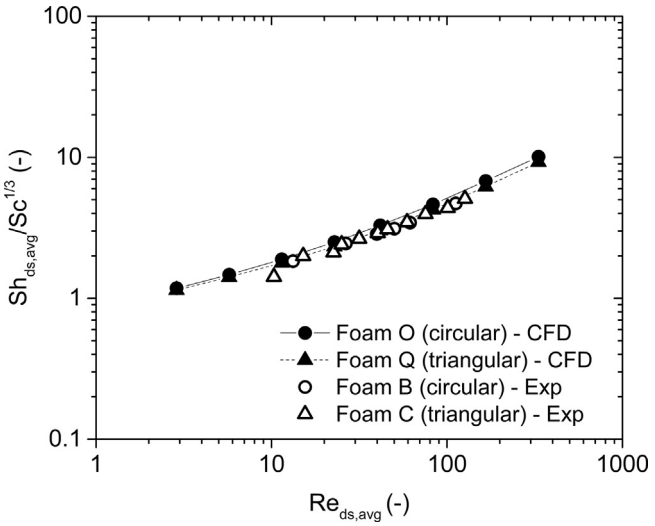

Fig. 9. Sherwood numbers versus Reynolds number for different foam samples. CFD simulations (full symbol) and experiments (empty symbol) carried out on circular (circle) and triangular (triangle) cross-sectional strut shape.

$$d_h = \frac{4\varepsilon}{S_v} \tag{14}$$

This choice of the length scale is directly inherited from the analysis of transport phenomena in honeycomb monoliths. It was originally defined for internal flows and can be directly employed for honeycomb monoliths because of the strong analogy between flow in monolith channels and in ducts. This choice is however improper for open-cell foams. The foam structure and the arrangement of the struts determine a nature of the flow which resembles flow around submerged objects rather than flow in channels. In this view, Reichelt et al. [28] have recently proposed the Sauter diameter (Eq. (15)) as the characteristic length. With this choice, the authors are trying to define a sphere-like diameter representative of the entire foam structure in an attempt to apply a packed bed correlation to the description of mass transfer in open-cell foams.

$$d_{Sauter} = \frac{6(1-\varepsilon)}{S_v} \tag{15}$$

The definition of the Sauter diameter requires the specific surface area of the foams. Reichelt et al. [28], however, do not explicitly define how to evaluate this pivotal property, which is taken directly from the relevant literature sources using in some case the value from tomograpy scans and in other cases estimates from different geometrical models.

When the Sauter diameter is used as the characteristic length in mass transfer correlation, we found a ± 50% scattering of data similar to that reported by Reichelt et al. [28]. On the other hand, according to our geometrical model, a quasi-linear relationship (Eq. (16)) exists between the average strut diameter and the ratio between the solid fraction and the specific surface area of foams.

$$d_{s,avg} \cong \frac{C(1-\varepsilon)}{S_v} \tag{16}$$

with different C values for circular ($C = 2.85$) and for triangular ($C = 4.86$) strut cross-sectional shape, respectively (additional details can be found in the Supplementary material, see Fig. S4).

Accordingly, an equivalent diameter approach can be used only by introducing a specific shape factor ($\Phi = C/6$), which accounts for the complex geometry and topology of open-cell foams, in the expression of a corrected equivalent diameter (Eq. (17)).

$$d_{eq,corr} = \Phi d_{Sauter} \cong d_{s,avg} \tag{17}$$

According to our geometrical model, we evaluate a shape factor equal to 0.475 and 0.810 for foams with circular and triangular strut cross-sectional shapes, respectively, which makes $d_{eq,corr}$ practically equivalent to the average strut size.

In conclusion, we adopt as characteristic length the average strut size which we consider the most physically sound length scale, being able to describe the complex flow nature phenomena in these structures

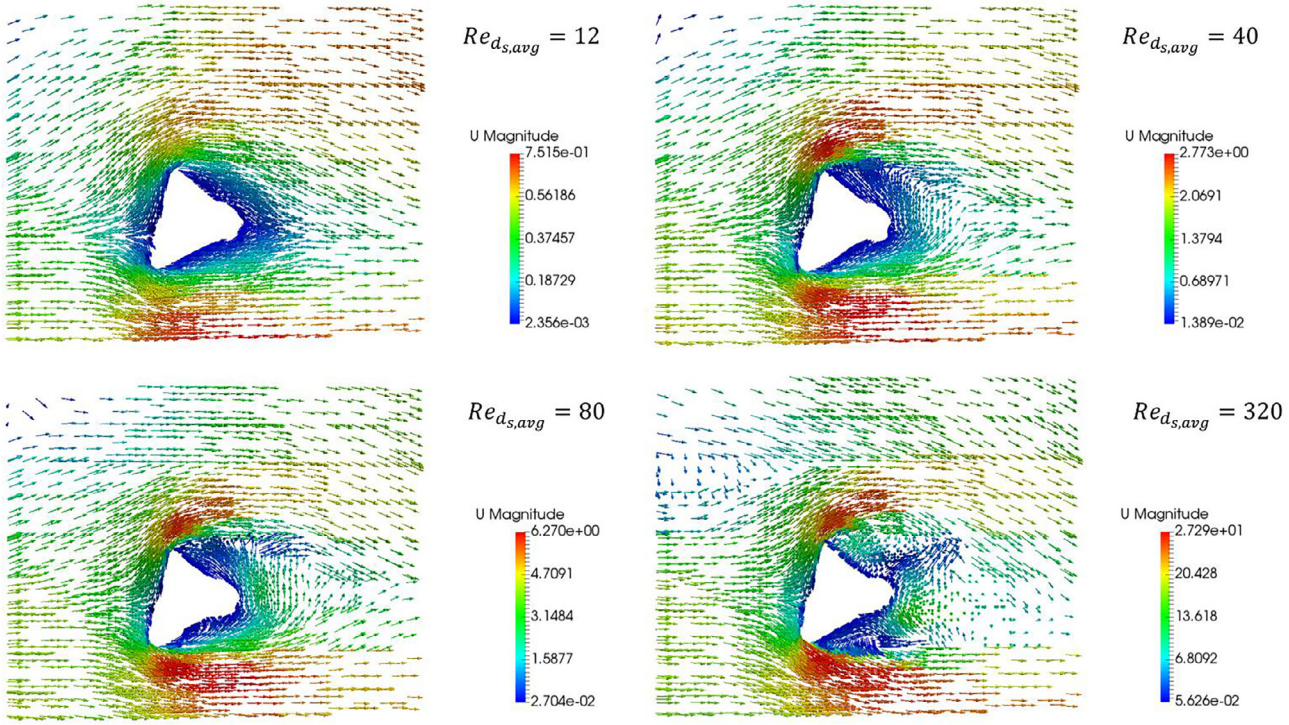

Fig. 10. Velocity vector around a strut in cross-flow at different Reynolds number for a foam of 2 mm of cell size and a porosity of 0.9. The vectors are colored as a function of the magnitude of the fluid velocity.

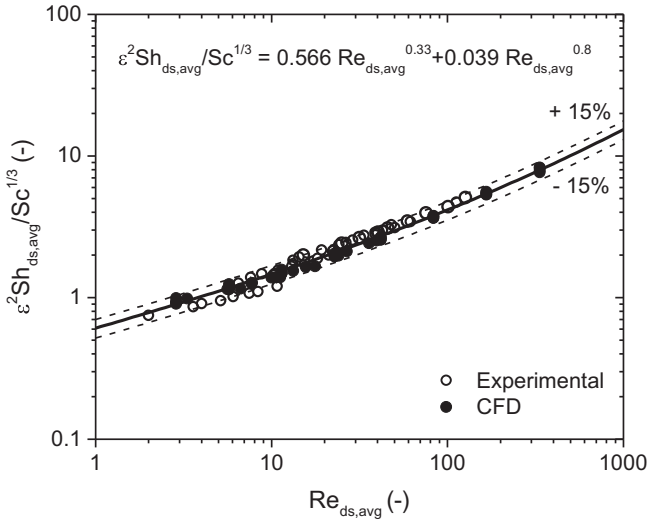

Fig. 11. Sherwood number as a function of the Reynolds number for experiments – this work and Giani et al. [1] – (empty symbol) and CFD simulation (full symbol) along with hereby proposed mass transfer correlation (full line).

Table 5
Geometrical properties of supports used for comparison of reactor sizes.

Foam sample	$d_{channel}/d_{cell}$ [mm]	ε/OFA [–]	S_v [m^{-1}]	Lc [mm]
900/2.5 Honeycomb	0.784	0.850	4355	0.847
Circular strut foam	0.600	0.900	3427	0.075
Triangular strut foam	0.600	0.950	3817	0.060

catching the transition between different flow regimes at the typical Reynolds numbers for cylinders in cross-flow. This choice has the noteworthy property to lead to a unified description of mass transfer in foams with both circular and triangular struts.

5.2. Mass transfer correlation

Several correlations have been proposed in the literature for external mass and heat transfer in open-cell foams. Usually, these correlations express the Sherwood number as a function of an appropriate Reynolds number and of the Schmidt number. The experimental and numerical studies carried out in this work have established that the convective mass transfer depends on the flow conditions and on the geometrical properties of open-cell foams as well. Along these lines, we account for the different flow regimes using two distinct asymptotic contributions, related to the creeping flow and to the post-Forchheimer regime, respectively, as already proposed in the context of open-cell foams by Reichelt et al. [28]. The fully laminar regime is modeled using a functional dependence of the dimensionless mass transfer coefficient on the Reynolds number raised to a power of 1/3. This relies on both the CFD simulations on the reconstructed foams (Section 4) and on the experimental tests carried out at low Reynolds numbers (Section 3). This result is confirmed by Ishimi et al. [39] who derived the same dependence in case of creeping viscous flow in periodic arrays of cylinders by the analytical solution of the governing equations. This exponent is close to the typical value assumed for heat transfer in tube banks at $10 < Re < 100$, which is 0.4 [49]. The second regime is described by a dependence on the Reynolds number raised to 0.8, typical of the fully turbulent regime in bundles of tubes [50]. Thus, the correlation assumes, therefore, the following functional form:

$$Sh_{d_{s,avg}} = (ARe_{d_{s,avg}}^{0.33} + BRe_{d_{s,avg}}^{0.8})Sc^{1/3} \tag{18}$$

Furthermore, the description of the mass transport phenomena requires accounting for the dependence on the porosity of the foam. According to the numerical simulations, we derived an empirical dependence on the inverse of the square of the void fraction. It is worth to emphasize that this dependence is also related to the adoption of the geometrical model for the evaluation of both specific surface area and average strut size. Thus, the hereby proposed correlation requires the estimation of these properties with the tetrakaidekahedral geometrical model proposed by Ambrosetti et al. [9]. The functional dependence on the Schmidt number is assumed to be the common raised to a power 1/3 [51]. The following correlation is accordingly the best representation of the external mass transfer based on both numerical simulations and experimental tests:

$$Sh_{d_{s,avg}} = \varepsilon^{-2}(0.566Re_{d_{s,avg}}^{0.33} + 0.039Re_{d_{s,avg}}^{0.8})Sc^{1/3} \tag{19}$$

The numerical coefficients are evaluated from the regression of both numerical and experimental tests. The hereby estimated coefficients of the mass transfer correlation deviate from the literature value for tube banks because of the different morphological structure of open-cell foams, which show struts randomly oriented and joined together in nodes. Fig. 11 shows experimental mass transfer runs both from this work and from Giani et al. [1] along with numerical CFD simulations plotted against Eq. (19). A good agreement is achieved with deviations below ± 15% for the prediction of the mass transfer coefficients. The applicability ranges of the hereby derived correlation are $1 < Re_{d_{s,avg}} < 300$, $0.7 < \varepsilon < 0.95$ and $0.3 < d_c < 5$ mm.

An analogous result is achieved by considering the foam equivalent diameter with proper shape factors as the characteristic length, see Fig. S5 in the Supplementary Material. Some deviations are observed at high

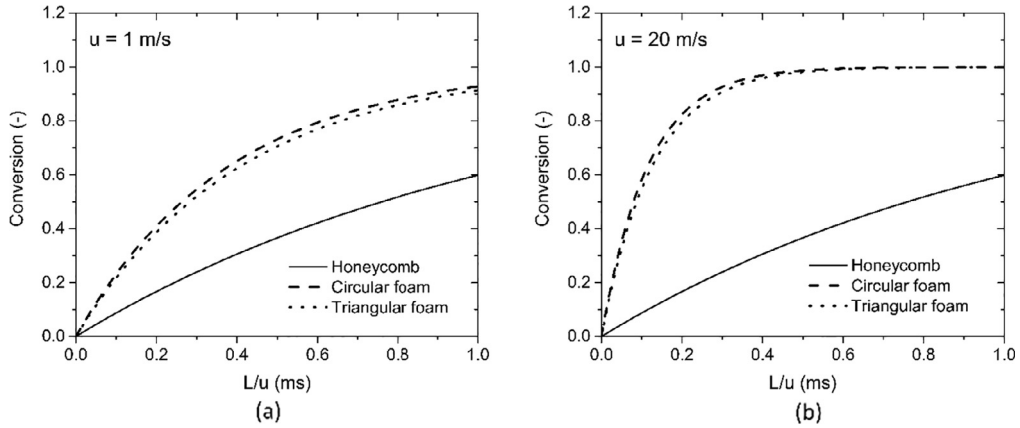

Fig. 12. Calculated external transfer limited conversion for honeycombs (solid line), circular strut foam (dashed line) and triangular strut foam (dotted line) versus the sample length for different fluid velocities: 1 m/s (a) and 20 m/s (b).

void fractions ($\varepsilon > 0.925$) where the average strut size and the equivalent diameter show some discrepancies.

5.3. Comparative analysis of the reactor size

Open-cell foams are considered as an enhanced catalyst support due to their potential to increase heat and mass transfer rates. This aspect is particularly attractive in view of the needs for process intensification in after-treatment devices, where space and weight limitations are quite stringent. In this paragraph, we compare the mass transfer performances of open-cell foams with those of state of the art honeycombs in terms of volumetric mass transfer coefficients by numerical calculations. The geometrical properties of the supports are reported in Table 5. Honeycombs are characterized by a Sherwood number that is constant and function of the channel geometry only, when the flow-field is laminar and minor entrance effects are neglected [52]. In this comparison, typical conditions of an after-treatment device are used for the evaluation of the relevant transport properties, considering CO combustion in air at 573 K and 1 bar. A state of the art square channel honeycomb substrate characterized by 900 channels per square inch (CPSI) and an open frontal area of 0.85 is chosen- (a standard 900/2.5 honeycomb). This support is compared with foams with circular and triangular struts characterized by a porosity equal to 0.9 and 0.95 respectively for the two different strut shapes. The cell diameter was equal to 600 μm, in line with the features of Foam A, i.e. a commercial material. Fig. 12 shows the calculated mass-transfer limited conversions against the residence time for two different flow velocities, namely a very low velocity of 1 m/s and a moderate velocity equal to 20 m/s, representative of a wide range of possible operating conditions in environmental applications. The conditions for the foam with circular struts correspond to Re equal to 1.5 and 30 respectively, the Reynolds number for the foam with triangular strut are equal to 1.2 and 24.

At low velocity, both the chosen foams outperform the state of the art honeycomb substrate. This is even more evident at the higher velocity, which enhances the mass transfer performances of the foams further widening the differences with the honeycomb. This result is caused by the different dependence of the mass transfer coefficients on the Reynolds number. Fig. 12 discloses the potential of these structures in the after-treatment field, where much more compact catalyst substrates could replace state of the art honeycombs. Notably, these applications are governed by the tradeoff between mass transfer performances and pressure drops, represented e.g. by the so-called merit index introduced in [1]. Further studies will be devoted to the analysis of pressure drops in foams for an extensive evaluation of the merit index in conditions of industrial relevance.

6. Conclusions

We have proposed a systematic investigation of the external mass transfer phenomena in open-cell catalytic foams based on a combined experimental and numerical approach. The hierarchical approach has been exploited for the analysis of this novel structured catalyst, proving its potential in the analysis of new reactor geometries. In particular, CFD simulations on virtually reconstructed foams have been exploited for the comprehensive investigation of the effects of the geometrical features of open-cell foams. The porosity mostly affects the mass transfer coefficients, which show a dependence on the inverse of the square of the void fraction. Conversely, the cell sizes and the cross-sectional shape of the struts have a negligible influence on the Sherwood number based on the average strut diameter. Dedicated experimental tests have been carried out both to extensively validate the numerical results and to extend the range of the analyzed samples in different flow regimes. Numerical and experimental results are jointly interpreted by means of a theoretically grounded geometrical model able to accurately describe both the specific surface area and the average strut size, i.e. the characteristic length. The insight in the flow field provided by CFD simulations points out that two distinct flow regimes are present. A creeping flow and an unsteady laminar flow regime prevail, depending on the Reynolds number. Moreover, the transition between the regimes is around the same literature value of Re as for flow around submerged objects. This supports the adoption of the average strut size as the characteristic length for foams, being able to fully capture the fluid dynamic features of the system. An engineering correlation combining the two asymptotic contributions has been derived which is able to describe the mass transfer coefficients as a function of the geometrical properties of the foams. Both the experimental data and the numerical simulations are accurately described with deviations at most of 15%. An alternative approach based on the use of an equivalent diameter as the characteristic length, showing almost equivalent fitting quality when including proper shape factors to describe the different cross-sectional features of the struts, has been also proposed and discussed.

On a more general basis, the design of novel structured reactors loaded with open-cell foam catalysts is simplified by the accurate description of the external mass transfer rates achieved in this work over an unprecedented range of conditions.

Acknowledgements

The research leading to these results has received funding from the European Research Council under the European Union's Horizon 2020 research and innovation program (Grant Agreement no. 694910/INTENT). Computational time at CINECA (Bologna, Italy) is gratefully acknowledged.

Appendix A. Supplementary data

Supplementary data associated with this article can be found, in the online version, at https://doi.org/10.1016/j.cej.2018.07.023.

References

[1] L. Giani, G. Groppi, E. Tronconi, Mass-transfer characterization of metallic foams as supports for structured catalysts, Ind. Eng. Chem. Res. 44 (2005) 4993–5002, https://doi.org/10.1021/ie0490886.
[2] L. Giani, G. Groppi, E. Tronconi, Heat transfer characterisation of metallic foams, Ind. Eng. Chem. Res. 44 (2005) 9078–9085.
[3] E. Bianchi, T. Heidig, C.G. Visconti, G. Groppi, H. Freund, E. Tronconi, Heat transfer properties of metal foam supports for structured catalysts: wall heat transfer coefficient, Catal. Today 216 (2013) 121–134, https://doi.org/10.1016/j.cattod.2013.06.019.
[4] E. Bianchi, T. Heidig, C.G. Visconti, G. Groppi, H. Freund, E. Tronconi, An appraisal of the heat transfer properties of metallic open-cell foams for strongly exo-/endothermic catalytic processes in tubular reactors, Chem. Eng. J. 198–199 (2012) 512–528, https://doi.org/10.1016/j.cej.2012.05.045.
[5] P.J. Jodłowski, Ł. Kuterasiński, R.J. Jędrzejczyk, D. Chlebda, A. Gancarczyk, S. Basąg, L. Chmielarz, DeNOx Abatement Modelling over Sonically Prepared Copper USY and ZSM5 Structured Catalysts, Catalysts. 7 (2017) 205, https://doi.org/10.3390/catal7070205.
[6] A. Donazzi, M. Maestri, B.C. Michael, A. Beretta, P. Forzatti, G. Groppi, E. Tronconi, L.D. Schmidt, D.G. Vlachos, Microkinetic modeling of spatially resolved autothermal CH4 catalytic partial oxidation experiments over Rh-coated foams, J. Catal. 275 (2010) 270–279, https://doi.org/10.1016/j.jcat.2010.08.007.
[7] R. Horn, N.J. Degenstein, K.A. Williams, L.D. Schmidt, Spatial and temporal profiles in millisecond partial oxidation processes, Catal. Letters. 110 (2006) 169–178, https://doi.org/10.1007/s10562-006-0117-8.
[8] T.T. Huu, M. Lacroix, C. Pham Huu, D. Schweich, D. Edouard, Towards a more realistic modeling of solid foam: use of the pentagonal dodecahedron geometry, Chem. Eng. Sci. 64 (2009) 5131–5142, https://doi.org/10.1016/j.ces.2009.08.028.
[9] M. Ambrosetti, M. Bracconi, G. Groppi, E. Tronconi, Analytical geometrical model of open cell foams with detailed description of strut-node intersection, Chemie-Ingenieur-Technik. 89 (2017), https://doi.org/10.1002/cite.201600173.
[10] A. Inayat, H. Freund, T. Zeiser, W. Schwieger, Determining the specific surface area of ceramic foams: the tetrakaidecahedra model revisited, Chem. Eng. Sci. 66 (2011) 1179–1188, https://doi.org/10.1016/j.ces.2010.12.031.
[11] G. Ambrosio, N. Bianco, W.K.S. Chiu, M. Iasiello, V. Naso, M. Oliviero, The effect of open-cell metal foams strut shape on convection heat transfer and pressure drop, Appl. Therm. Eng. 103 (2016) 333–343, https://doi.org/10.1016/j.applthermaleng.2016.04.085.
[12] M. Zafari, M. Panjepour, M.D. Emami, M. Meratian, Microtomography-based numerical simulation of fluid flow and heat transfer in open cell metal foams, Appl.

Therm. Eng. 80 (2015) 347–354, https://doi.org/10.1016/j.applthermaleng.2015.01.045.
[13] S. Meinicke, T. Wetzel, B. Dietrich, Scale-resolved CFD modelling of single-phase hydrodynamics and conjugate heat transfer in solid sponges, Int. J. Heat Mass Transf. 108 (2017) 1207–1219, https://doi.org/10.1016/j.ijheatmasstransfer.2016.12.052.
[14] M. Bracconi, M. Ambrosetti, M. Maestri, G. Groppi, E. Tronconi, A systematic procedure for the virtual reconstruction of open-cell foams, Chem. Eng. J. 315 (2017) 608–620, https://doi.org/10.1016/j.cej.2017.01.069.
[15] G.D. Wehinger, H. Heitmann, M. Kraume, An artificial structure modeler for 3D CFD simulations of catalytic foams, Chem. Eng. J. 284 (2016) 543–556, https://doi.org/10.1016/j.cej.2015.09.014.
[16] Z. Nie, Y. Lin, Q. Tong, Numerical investigation of pressure drop and heat transfer through open cell foams with 3D Laguerre-Voronoi model, Int. J. Heat Mass Transf. 113 (2017) 819–839, https://doi.org/10.1016/j.ijheatmasstransfer.2017.05.119.
[17] J. Von Rickenbach, F. Lucci, C. Narayanan, P. Dimopoulos Eggenschwiler, D. Poulikakos, Multi-scale modelling of mass transfer limited heterogeneous reactions in open cell foams, Int. J. Heat Mass Transf. 75 (2014) 337–346, https://doi.org/10.1016/j.ijheatmasstransfer.2014.03.060.
[18] F. Lucci, A. Della Torre, J. von Rickenbach, G. Montenegro, D. Poulikakos, P. Dimopoulos Eggenschwiler, Performance of randomized Kelvin cell structures as catalytic substrates: mass-transfer based analysis, Chem. Eng. Sci. 112 (2014) 143–151, https://doi.org/10.1016/j.ces.2014.03.023.
[19] S. De Schampheleire, P. De Jaeger, K. De Kerpel, B. Ameel, H. Huisseune, M. De Paepe, How to study thermal applications of open-cell metal foam: experiments and computational fluid dynamics, Materials (Basel). 9 (2016) 1–27, https://doi.org/10.3390/ma9020094.
[20] A. Della Torre, F. Lucci, G. Montenegro, A. Onorati, P. Dimopoulos Eggenschwiler, E. Tronconi, G. Groppi, CFD modeling of catalytic reactions in open-cell foam substrates, Comput. Chem. Eng. 92 (2016) 55–63, https://doi.org/10.1016/j.compchemeng.2016.04.031.
[21] W. Peng, M. Xu, X. Li, X. Huai, Z. Liu, H. Wang, CFD study on thermal transport in open-cell metal foams with and without a washcoat: effective thermal conductivity and gas-solid interfacial heat transfer, Chem. Eng. Sci. 161 (2017) 92–108, https://doi.org/10.1016/j.ces.2016.12.006.
[22] T. Heidig, T. Zeiser, H. Freund, Influence of resolution of rasterized geometries on porosity and specific surface area exemplified for model geometries of porous media, Transp. Porous Media. 120 (2017) 207–225, https://doi.org/10.1007/s11242-017-0916-y.
[23] P. Habisreuther, N. Djordjevic, N. Zarzalis, Statistical distribution of residence time and tortuosity of flow through open-cell foams, Chem. Eng. Sci. 64 (2009) 4943–4954, https://doi.org/10.1016/j.ces.2009.07.033.
[24] M.V. Twigg, J.T. Richardson, Fundamentals and applications of structured ceramic foam catalysts, Ind. Eng. Chem. Res. 46 (2007) 4166–4177, https://doi.org/10.1021/ie061122o.
[25] G. Groppi, L. Giani, E. Tronconi, Generalized correlation for gas/solid mass-transfer coefficients in metallic and ceramic foams, Ind. Eng. Chem. Res. 46 (2007) 3955–3958, https://doi.org/10.1021/ie061330g.
[26] G. Incera Garrido, F.C. Patcas, S. Lang, B. Kraushaar-Czarnetzki, Mass transfer and pressure drop in ceramic foams: a description for different pore sizes and porosities, Chem. Eng. Sci. 63 (2008) 5202–5217, https://doi.org/10.1016/j.ces.2008.06.015.
[27] B. Dietrich, Heat transfer coefficients for solid ceramic sponges–experimental results and correlation, Int. J. Heat Mass Transf. 61 (2013) 627–637, https://doi.org/10.1016/j.ijheatmasstransfer.2013.02.019.
[28] E. Reichelt, M. Jahn, Generalized correlations for mass transfer and pressure drop in fiber-based catalyst supports, Chem. Eng. J. 325 (2017) 655–664, https://doi.org/10.1016/j.cej.2017.05.119.
[29] S. Rebughini, A. Cuoci, M. Maestri, Hierarchical analysis of the gas-to-particle heat and mass transfer in micro packed bed reactors, Chem. Eng. J. 289 (2016) 471–478, https://doi.org/10.1016/j.cej.2015.12.089.
[30] S. Rebughini, M. Bracconi, A.G. Dixon, M. Maestri, A hierarchical approach to chemical reactor engineering: an application to micro packed bed reactors, React. Chem. Eng. 3 (2018) 25–33, https://doi.org/10.1039/C7RE00195A.
[31] R. Balzarotti, C. Cristiani, L.F. Francis, Spin coating deposition on complex geometry substrates: Influence of operative parameters, Surf. Coatings Technol. (2017), https://doi.org/10.1016/j.surfcoat.2017.09.077.
[32] M. Maestri, A. Cuoci, Coupling CFD with detailed microkinetic modeling in heterogeneous catalysis, Chem. Eng. Sci. 96 (2013) 106–117, https://doi.org/10.1016/j.ces.2013.03.048.
[33] S.A. Logtenberg, M. Nijemeisland, A.G. Dixon, Computational fluid dynamics simulations of fluid flow and heat transfer at the wall-particle contact points in a fixed-bed reactor, Chem. Eng. Sci. 54 (1999) 2433–2439, https://doi.org/10.1016/S0009-2509(98)00445-X.
[34] R.K. Shah, A.L. London, Laminar Flow Forced Convection in Ducts: A Source Book for Compact Heat Exchanger Analytical Data, Academic press, 1978.
[35] A. Cuoci, A. Frassoldati, T. Faravelli, E. Ranzi, OpenSMOKE++: an object-oriented framework for the numerical modeling of reactive systems with detailed kinetic mechanisms, Comput. Phys. Commun. 192 (2015) 237–264, https://doi.org/10.1016/j.cpc.2015.02.014.
[36] S. Gordon, B.J. McBride, Computer program for calculation of complex chemical equilibrium compositions and applications, National Aeronautics and Space Administration, Office of Management, Scientific and Technical Information Program, 1994.
[37] J. Hirschfelder, R.B. Bird, C.F. Curtiss, Molecular Theory of Gases and Liquids, Wiley, 1964.
[38] C.F. Curtiss, J.O. Hirschfelder, Transport properties of multicomponent gas mixtures, J. Chem. Phys. 17 (1949) 550–555, https://doi.org/10.1063/1.1747319.
[39] K. Ishimi, S. Koroyasu, H. Hikita, Mass transfer in creeping flow past periodic arrays of cylinders, J. Chem. Eng. Japan. 20 (1987) 492–498, https://doi.org/10.1252/jcej.20.492.
[40] J. Happel, H. Brenner, Viscous flow in multiparticle systems: motion of spheres and a fluid in a cylindrical tube, AIChE J. 3 (1957) 506–513, https://doi.org/10.1002/aic.690030415.
[41] E. Brun, J. Vicente, F. Topin, R. Occelli, M.J. Clifton, Microstructure and transport properties of cellular materials: representative volume element, Adv. Eng. Mater. 11 (2009) 805–810, https://doi.org/10.1002/adem.200900131.
[42] R. Pfeffer, Heat and mass transport in multiparticle systems, Ind. Eng. Chem. Fundam. 3 (1964) 380–383, https://doi.org/10.1021/i160012a018.
[43] B. Dietrich, Pressure drop correlation for ceramic and metal sponges, Chem. Eng. Sci. 74 (2012) 192–199, https://doi.org/10.1016/j.ces.2012.02.047.
[44] O. Zeitoun, M. Ali, A. Nuhait, Convective heat transfer around a triangular cylinder in an air cross flow, Int. J. Therm. Sci. 50 (2011) 1685–1697, https://doi.org/10.1016/j.ijthermalsci.2011.04.011.
[45] H. Abbassi, S. Turki, S. Ben Nasrallah, Numerical investigation of forced convection in a plane channel with a built-in triangular prism, Int. J. Therm. Sci. 40 (2001) 649–658, https://doi.org/10.1016/S1290-0729(01)01254-6.
[46] A. Della Torre, G. Montenegro, G.R. Tabor, M.L. Wears, CFD characterization of flow regimes inside open cell foam substrates, Int. J. Heat Fluid Flow. 50 (2014) 72–82, https://doi.org/10.1016/j.ijheatfluidflow.2014.05.005.
[47] M. Bracconi, M. Maestri, A. Cuoci, In situ adaptive tabulation for the CFD simulation of heterogeneous reactors based on operator-splitting algorithm, AIChE J. 63 (2017) 95–104, https://doi.org/10.1002/aic.15441.
[48] A. Inayat, M. Klumpp, M. Lämmermann, H. Freund, W. Schwieger, Development of a new pressure drop correlation for open-cell foams based completely on theoretical grounds: taking into account strut shape and geometric tortuosity, Chem. Eng. J. 287 (2016) 704–719, https://doi.org/10.1016/j.cej.2015.11.050.
[49] T.L. Bergman, F.P. Incropera, Fundamentals of Heat and Mass Transfer, Wiley, 2011.
[50] V. Gnielinski, Equations for calculating heat transfer in single tube rows and banks of tubes in transverse flow, Int. Chem. Eng. 19 (1979) 3.
[51] R.B. Bird, W.E. Stewart, E.N. Lightfoot, Transport Phenomena, Revised 2nd Edition, 2nd ed., John Wiley & Sons Inc, 2006.
[52] E. Tronconi, P. Forzatti, Adequacy of lumped parameter models for SCR reactors with monolith structure, AIChE J. 38 (1992) 201–210, https://doi.org/10.1002/aic.690380205.